Microneedle-assisted microparticle delivery by gene guns: experiments and modeling on the effects of particle characteristics.

Microneedle Assisted Micro-particle Delivery by Gene Guns: Experiments and Modelling on the Effects of Particle Characteristics

Dongwei Zhang, Chris D Rielly, Diganta B Das*

Department of Chemical Engineering, Loughborough University, Loughborough LE113TU, UK

Short title: Microneedle Assisted Micro-particle Delivery

*Corresponding author; Email: d.b.das@lboro.ac.uk

Microneedle Assisted Micro-particle Delivery by Gene Guns: Experiments and Modelling on the Effects of Particle Characteristics

Dongwei Zhang, Chris D Rielly, Diganta B Das*

Department of Chemical Engineering, Loughborough University, Loughborough LE113TU, UK

(*Corresponding author; Email: d.b.das@lboro.ac.uk)

Abstract

Microneedles (MNs) have been shown to enhance the penetration depths of micro-particles delivered by gene gun. This paper aims to investigate the penetration of model micro-particle materials, namely, tungsten (< 1 μm diameter) and stainless steel (18 and 30 μm diameters) into a skin mimicking agarose gel to determine the effects of particle characteristics (mainly particle size). A number of experiments have been processed to analyse the passage percentage and the penetration depth of these micro-particles in relation to the operating pressures and MN lengths. A comparison between the stainless steel and tungsten micro-particles has been discussed, e.g. passage percentage, penetration depth. The passage percentage of tungsten micro-particles is found to be less than the stainless steel. It is worth mentioning that the tungsten micro-particles present unfavourable results which show that they cannot penetrate into the skin mimicking agarose gel without the help of MN due to insufficient momentum due to the smaller particle size. This condition does not occur for stainless steel micro-particles. In order to further understand the penetration of the micro-particles, a mathematical model has been built based on the experimental set up. The penetration depth of the micro-particles is analysed in relation to the size, operating pressure and MN length for conditions which cannot be obtained in the experiments. In addition, the penetration depth difference between stainless steel and tungsten micro-particles is studied using the developed model to further understand the effect of an increased particle density and size on the penetration depth.

Key words: Gene gun, microneedle, micro-particles, micro-particle density, micro-particle size, penetration depth, passage percentage

1. Introduction

Gene gun systems have been designed primarily as needle free techniques which can accelerate DNA loaded micro-particles to provide sufficient momentum so that they can breach the outer layer of the skin and achieve the purposes of gene transfection (Kis et al., 2012; Soliman, 2011; Walters et al., 2007; Kendall et al., 2004). Generally, the epidermis layer of the skin is considered as the main target of these micro-particles (Soliman et al., 2011; Liu, 2006; Quinlan et al., 2001; Bennett et al., 1999; Trainer et al., 1997). However, cell and tissue damages are particular problems for the use of gene guns (Obrien et al., 2011; Uchida et al., 2009; Thomas et al., 2001; Sato et al., 2000; Yoshida et al., 1997). In principle, reduction of the operation pressure in the gene guns (Xia et al., 2011; Uchida et al. 2009; Yoshida et al., 1997) and particle size (Obrien et al.,

38   2011) can minimize the cell/tissue damage but these tend to decrease the particle momentum and, hence,

39   the penetration depths of the micro-particles in the tissue. In order to resolve these issues, a series of

40   experiments which combine solid microneedles (MNs) with an in-house micro-particle delivery system (see

41   Figure 1) has been reported recently by Zhang et al. (2013a,2014). The potential of a system that combines

42   microneedles and gene guns has been discussed in details by Zhang et al. (2013b).

43

44   MNs are minimally invasive microstructures that can pierce the outer layer of skin, namely the *stratum*

45   *corneum*, almost painlessly which has been shown to enhance drug delivery rate (e.g., Olatunji and Das,

46   2011; Nayak et al., 2013; Olatunji et al., 2013; Donnelly et al., 2012). They are generally classified into 'solid'

47   and 'hollow' microneedles (e.g., Al-Qallaf et al., 2009; Olatunji and Das, 2010; Olatunji et al., 2012; Nayak

48   and Das, 2013; Han and Das, 2013; Zhang et al., 2013a,b). The solid MNs are able to penetrate the human

49   skin to make holes (Kalluri et al., 2011; Davis et al., 2004; McAllister et al., 2003) as well as deliver

50   drugs/genes which are coated (Cormier et al., 2004) or encapsulated (Miyano et al., 2005). The MN holes

51   can also be used by the biolistic system for the delivery of the micro-particles. In this case, the micro-particles

52   can penetrate with less resistance into the skin through the holes and further achieve an enhanced

53   penetration depth to allow gene transfection in deeper tissue. Zhang et al. (2014) have used the experimental

54   setup of MN assisted micro-particle delivery to fire biocompatible stainless steel micro-particles having an

55   average diameter of 18 μm into a skin mimicking agarose gel. Their results have shown that a number of

56   micro-particles penetrate through the holes and achieve a considerable increase in the maximum penetration

57   depth, e.g., a penetration depth of 1272 ± 42 μm was achieved inside the gel using 1500 μm long MNs

58   (AdminPatch MN 1500) as compared to the cases where the same gel and operating conditions were used

59   and yet little or no penetration of MNs was observed due to the absence of MNs.

60

61   The overall process of MN assisted transdermal micro-particle delivery from gene guns consists of three main

62   stages, which are the acceleration, separation and deceleration stages (Zhang et al., 2013a, 2014). These

63   stages are identified in Figure 1. As can be seen, the experimental set up stores the pressurized gas in a gas

64   receiver to a desired pressure which is detected by a digital pressure transducer. The release of the

65   pressurized gas is operated by a solenoid valve. In addition, it is worth mentioning that the system uses a

66   ground slide which can prevent the impact of pressurized gas on the target tissue and release the gas from

67   the ventholes in the barrel. The acceleration stage is a major part of the particle delivery process as it is within

68   this stage the micro-particles are accelerated to sufficient velocities using the pressurized gas as a driving

69   source. To achieve these, the micro-particles are compressed and bound loosely into a pellet form and

70   loaded into a ground slide in the system (Figure 1). As the ground slide is accelerated by the pressurised gas,

71   the pellet containing the micro-particles is also accelerated. The separation stage is then followed which is

72   aimed at separating the pellet into individual particles by a mesh although it is possible that this stage

73   produces a few agglomerates.

74

75 The deceleration stage involves two steps as follows: (i) the transport of the micro-particles in a space

76 between mesh and target and (ii) the penetration of micro-particles into the chosen target. Previously, Zhang

77 et al. (2014) used an experimental rig (Figure 1) to deliver stainless steel micro-particles into a skin mimicking

78 agarose gel so as to demonstrate the feasibility of MN assisted micro-particle delivery. The results have

79 shown that an enhanced penetration depth of micro-particles inside the agarose gel can be achieved using

80 MN assisted micro-particle delivery at a much lower injection pressure compared to typical gene guns.

81

82 Generally, the route of the micro-particle penetration in the target tissue is divided into two types which are

83 the extracellular and intercellular routes (Zhang et al., 2013b; Soliman and Abdallah, 2011; Mitchell et al.,

84 2003). The extracellular route may occur with large particles due to failures between the cell boundaries

85 (Soliman, 2011). For example, Mitchell et al. (2003) have fired stainless steel micro-particles of 25 μm

86 average diameter into canine buccal mucosa using light gas gun (Crozier et al., 1957), which is governed by

87 the micro-particle transport through extracellular route. However, the disadvantage of this is that large particle

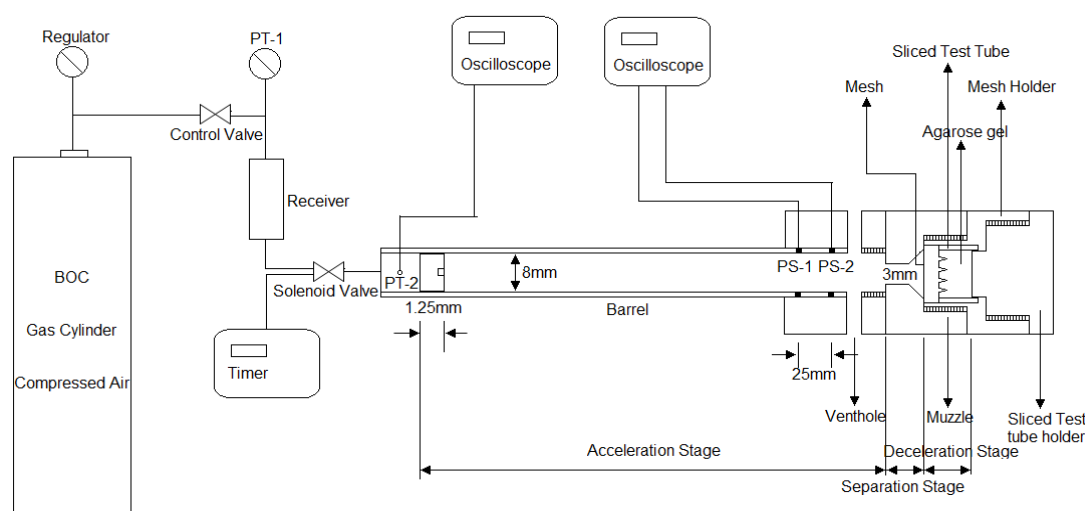88 sizes may cause a lot of damage or destroy the skin surface.

89

90 Figure 1: A schematic diagram of the experimental rig for the MN assisted micro-particle delivery system

91 (Zhang et al., 2014)

92

93 The intercellular route is considered to be important in the case of delivering small particles, which pass

94 through individual cell membranes, e.g., it can be used for particle mediated DNA immunization (Soliman and

95 Abdallah, 2011; Hardy et al., 2005). Dense materials (e.g. gold and tungsten) are often made into small

96 particles of a diameter ranging from 0.6 to 6 μm (Soliman, 2011; Hardy et al., 2005) which are smaller than

97 typical cell diameters. The particles can be accelerated to higher speeds to obtain enough momentum to

98 breach the skin and penetrate through the individual cell membranes. Although gold is recommended for the

99 particle delivery due to its high density, low toxicity and lack of chemical reactivity (Macklin, 2000), it is an

100 expensive material. Several studies for the golden micro-particles delivery have been made, which show that

101 the gold micro-particles can breach the human skin and penetrate to a depth ranging from 35 - 135 µm at 30

102 bar operating pressure (Arora et al., 2008; Giudice et al., 2006). Kendall et al. (2004) have used a

103 convergent-divergent device to accelerate gold particles of 1.8 µm diameter which achieve a maximum

104 penetration depth of 78.6 µm in the skin at 60 bar pressure. Mitchell et al. (2003) have found that gold particle

105 of 1 - 3 µm diameter can reach a depth of around 60 µm in canine tissue at an injection particle velocity of 550

106 ± 50 m/s. Recently, O'Brien et al. (2011) have reported that the penetration depth of golden micro-particles of

107 1 µm diameter in mouse ear tissue is 50 ± 11 µm when the Helios gene gun is used at an operating pressure

108 of 5.1 bar (75 psi).

109

110 In general, the intercellular route is the preferred penetration route due to less cell and tissue damages for the

111 small micro-particles. In order to validate the effect of the MN assisted micro-particle delivery on the small

112 micro-particles, tungsten micro-particles may be chosen to analyse the penetration in the skin mimicking

113 agarose gel. Tungsten micro-particles are considered to be a good substitute for golden micro-particles for

114 research of biolistic micro-particle delivery because of their cost effectiveness compared to gold particles,

115 despite the fact they can be toxic to cells (Bastian et al, 2009; Yoshimisu et al, 2009; Russell et al, 1992). For

116 example, Klein et al. (1987) first used a particle gun to accelerate spherical tungsten particles of 4 µm

117 diameter into epidermal cells of onions. Williams et al. (1991) have used a helium-driven apparatus to study

118 3.9 µm average diameter tungsten and of golden particles, with a diameter ranged from 2 to 5 µm, on mouse

119 liver. Recently, the review paper by Zhang et al. (2013b) has discussed the importance of particle

120 characteristics and operation condition on the delivery of the micro-particles in detail.

121

122 Motivated by the above work, this paper aims to investigate the effects of particle characteristics on MN

123 assisted micro-particle delivery by using micro-particles (e.g., tungsten micro-particles, biomedical grade

124 stainless steel) of different densities and particle sizes. The study also gives an indirect comparison between

125 the extracellular and intercellular routes using MN assisted micro-particle delivery. Zhang et al. (2013a)

126 determined the passage percentage of stainless steel micro-particles at various conditions, e.g., mesh pore

127 size, Polyvinylpyrrolidone (PVP - binder) concentration and operating pressure. They pointed out the required

128 mesh pore size and PVP concentration of pellets for MN assisted micro-particle delivery for given particle size.

129 This paper aims to revisit the same questions to determine the dependence of particle characteristics using

130 tungsten and stainless steel micro-particles with the help of Zhang et al. (2014)'s experimental rig. A skin

131 mimicking agarose gel is used as a target to determine the difference in penetration depth between tungsten

132 and stainless steel micro-particles. In order to further understand the particle size and density effect on the

133 penetration depth, a mathematical model of MN assisted micro-particle delivery is built using MATLAB

134 (Version R2012b). The mathematical model is used to analyse the theoretical penetration depth of those two

135 materials of micro-particles and further to verify the experimental results. In addition, the model aims to

136 investigate the effect of a range of target properties (e.g. density, viscosity) on the maximum penetration

depth of micro-particles. The developed model is also used to determine the characteristics of the micro-particle delivery where experimental data are not available. Please note that the paper is focused on modelling the micro-particle delivery process. The issues related to the loading of genes on these particles and subsequent gene transfection in a target cells are not discussed in this paper.

Please note that most of the technologies for loading DNA onto the particles and delivering the DNA-loaded particles are well developed. In the present context, we do not propose any changes to these existing methods but suggest a modification where the particle delivery process/devices are coupled with microneedles. The potential of these method are discussed in detail by Zhang et al. (2013a,b) and Zhang et al. (2014).

2. Materials and experimental methods

2.1 Materials

Irregular shaped tungsten micro-particles were purchased form Sigma-Aldrich Company Ltd (Gillingham, UK). It is considered as a good replacement for gold particles because its density is similar to gold and has a low cost (Menezes et al., 2012). Stainless steel mesh with pore size of 122 μm was obtained from MeshUK, Streme Limited (Marlow, UK). Irregular shaped and spherical biocompatible stainless steel micro-particles were purchased from Goodfellow Cambridge Ltd. (Huntingdon, UK) and LPW Technology Ltd. (Daresbury, UK), respectively. Agarose powder (Sigma-Aldrich Company Ltd., Gillingham, UK) was used to prepare a skin mimicking agarose gel which was used a target for the micro-particles penetration experiments. Detailed method of preparation for this gel is given by Zhang et al. (2014).
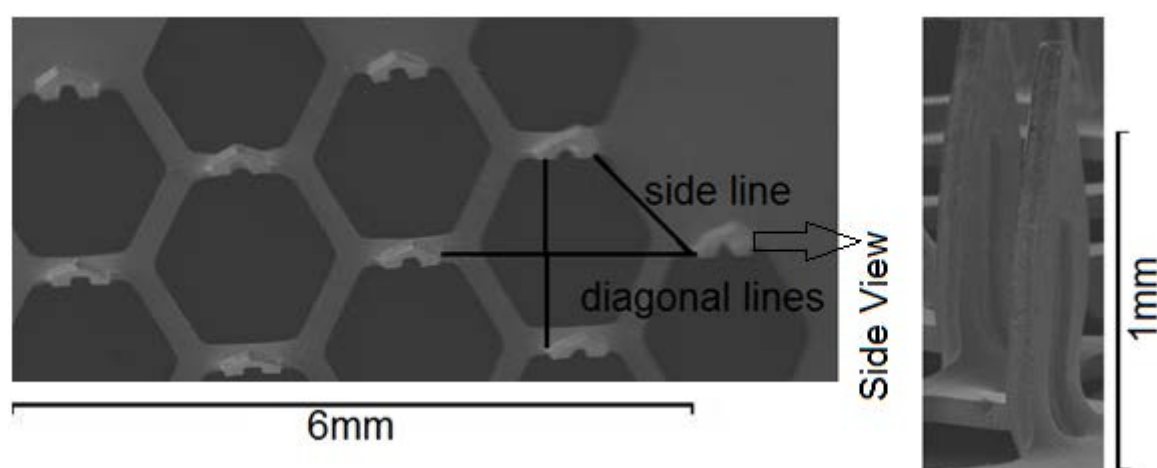

Figure 2: The image of AdminPatch 1500 (Note: MNs of AdminPatch 1200 are distributed as a diamond pattern) (Zhang et al., 2014)

Two different solid MN arrays which vary in the lengths of the MNs (AdminPatch 1200 and 1500) were purchased from nanoBioSciences limited liability company (Sunnyvale, CA, USA). The MNs are distributed as a diamond shape (see Figure 2) on a 1 cm^2 circular area. In addition, an in-house fabricated MN array is

used which consists of 750 μm long MNs. The characteristic of each MN array is presented in Table 1. Although the results from the use of different MNs may be different, a range of dimensions of the MNs provide us the opportunity to understand the effects of a geometric parameter more accurately. Therefore, we consider it to be important to use more than one MN in our experiments despite differences in their geometries.

2.2 Characterization of tungsten micro-particles

The particle size distribution of tungsten powder is analysed by a particle size analyser (Mastersizer 2000, Malvern Instruments, Ltd, Malvern, Worcestershire, UK). It is found to range from 0.198 to 1.439 μm with a mean diameter of 0.58 μm and Sauter mean diameter of 0.49 μm. The particles can be viewed in the SEM image in Figure 3. The tungsten particles are highly agglomerated and have rough surfaces. From the SEM image, 50 random micro-particles are chosen to measure the average sphericity of the tungsten micro-particles which is found to be 0.66 ± 0.13 μm. The average bulk density and porosity of tungsten powder are 7.43 ± 0.08 g/cm^3 and 59.6 ± 0.4%. Ultimately, by combining the SEM image results with the size distribution, gained from particle size analyser it is possible to confirm that the tungsten particles are a nano-size powder.

Table 1: The characterizations of the MN array (Zhang et al., 2014)

MN Name	Parameters	Value (μm)
Adminpatch MN 1500	Length	1500
	Width	480
	Thickness	78
	Space between MNs	1546
	Spaces on diagonal directions (see Figure 2)	1643
		3000
Adminpatch MN 1200	Length	1200
	Width	480
	Thickness	78
	Space between MNs	1252
	Spaces on diagonal directions	1970
		2426
In-house fabricated MN 750	Length	750
	Diameter	250
	Space between MNs	500

2.3 Characterization of the pellet

For the MN assisted micro-particle delivery, the micro-particles are required to be in the form a compressed cylindrical pellet which is prepared by a pellet press as described by Zhang et al. (2013a). Furthermore, the packing density should be homogeneous within the pellet as far as possible so as to increase the possibility that when the pellet is broken into particles and one obtains uniformly separated particles. This is an

189 important characteristic of the developed process. Heterogeneity in the packing of the pellet is likely to create

190 more uncertainty in the distribution of the separated particles. To prepare the cylindrical pellet, Zhang et al.

191 (2013a) have mixed 40 mg of PVP in 1 ml of ethanol in which an amount of 0.035 g stainless steel

192 micro-particles has been added and bind the particles together. The mixture is transferred to a pellet press

193 (Zhang et al., 2013a) and compressed into a solid cylindrical pellet. Ethanol is evaporated due to their high

194 volatility and therefore, it is not present in the dry pellet which is used in experiments. A similar method was

195 followed to produce the pellets in this work. Furthermore, the homogeneity of the micro-particle packing was

196 checked using a micro computed tomography (micro-CT). Micro-CT is an advanced non-destructive 3D

197 imaging technique which can be used to clearly understand the internal microstructure of the samples

198 (Ritman, 2004). Micro-CT has been used to detect any internal damage (e.g., internal fracture in the porous

199 pellet) and/or heterogeneity in the packing of pellet in this work. As an example, a three dimensional view of

200 the stainless steel pellet is shown in Figure 4a. As can be seen, the stainless steel micro-particles are

201 compressed into a homogenous cylindrical pellet with approximately 2 mm in diameter and length. Although

202 the top and button surfaces of the pellet are slightly uneven because the pellet gets stuck on the pellet press,

203 it is not a big concern as it seems the packing density of the particles does not vary. The internal top view of

204 the pellet at the position of 1.08 mm on the z axis is shown in Figure 4b and the size view of the internal

205 structure of the pellet at the position of 1.08 mm on the y-axis is shown in Figure 4c. It shows that PVP (white

206 spots) is non-uniformly distributed in the pellet. PVP fills the void space in the micro-particles causing them to

207 bind loosely together as indicated by the white circles (PVP) in the Figure 4b-c. The above figures cannot

208 clearly show the PVP combination of the pellet. Therefore an SEM view is provided which show the top
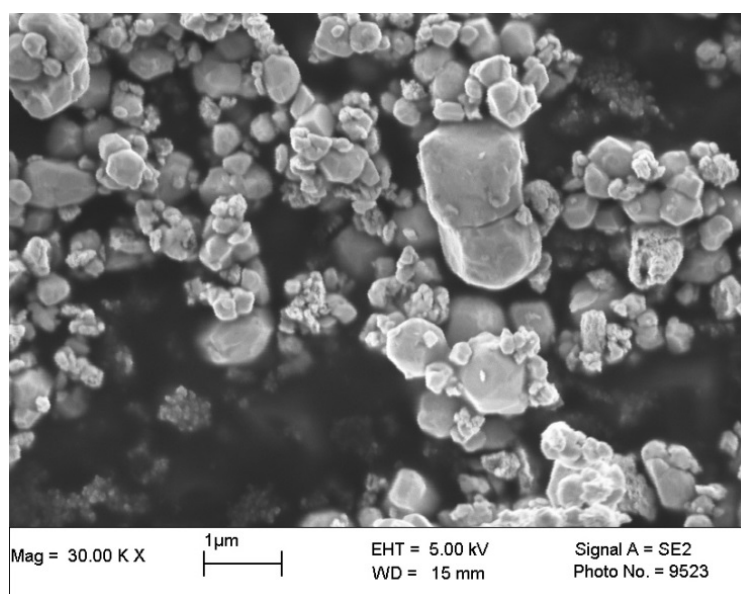
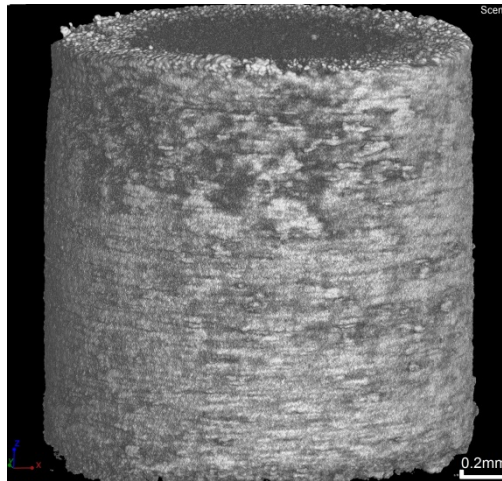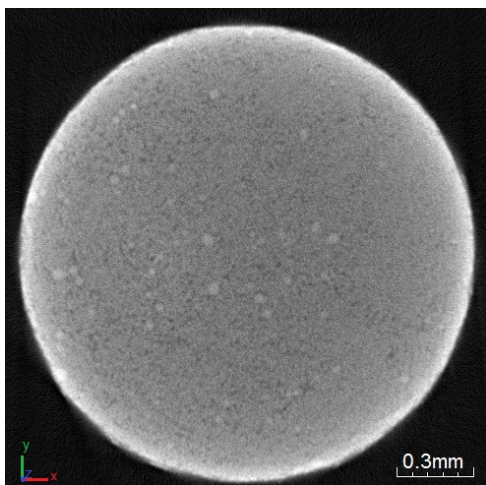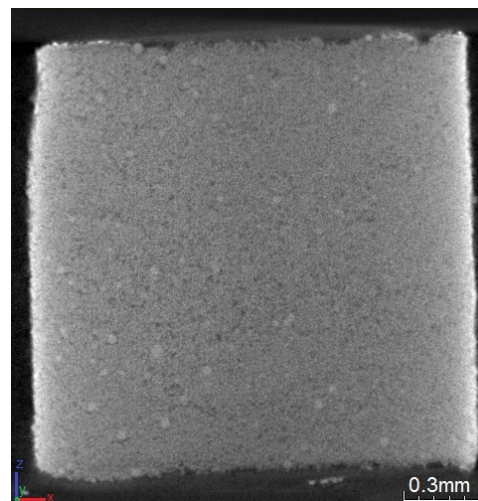209 surface of a pellet (see Figure 5a).

210   Figure 3: A SEM image of irregular tungsten powder (Sauter mean diameter: 0.49 µm)

211

212

(a)

(b)

(c)

Figure 4: Micro-CT images of a stainless steel micro-particle pellet made of 40 mg/ml PVP (white spots in the images): (a) reconstructed three dimension view of the pellet (b) top internal view across the pellet at the position of 1.08 mm on the z axis (c) side internal view across the pellet at the position of 1.08 mm on the y axis. The images show homogeneity of the packing of the micro-particles.

Figure 5(a) clearly shows the characterization of the pellet top surface. As can be seen, the micro-particles are bound to form a uniform pellet surface. As expected, the PVP is distributed non-uniformly around the pellet, which agrees with results detected by the micro-CT (Figure 4). Thus, it may cause the pellet to separate into a few agglomerates after the separation stage due to increased bind strength between some of micro-particles. Previously, Zhang et al. (2013a) have analysed the passage percentage of the pellet and size distribution of the separated particles using various operating pressure and different binder (PVP) concentration. They show that 40 mg/ml PVP in a pellet is ideal as it almost separates the pellet into individual micro-particles with some small agglomerates using 178 μm pore size of mesh. As presented in the Figure 5b, the application of mesh pore size presents a good control of the size distribution of the separated micro-particles and uses to the following experiments for the investigation of the penetration depth of

241   tungsten micro-particles in the skin mimicking agarose gel.

242

243   (a)

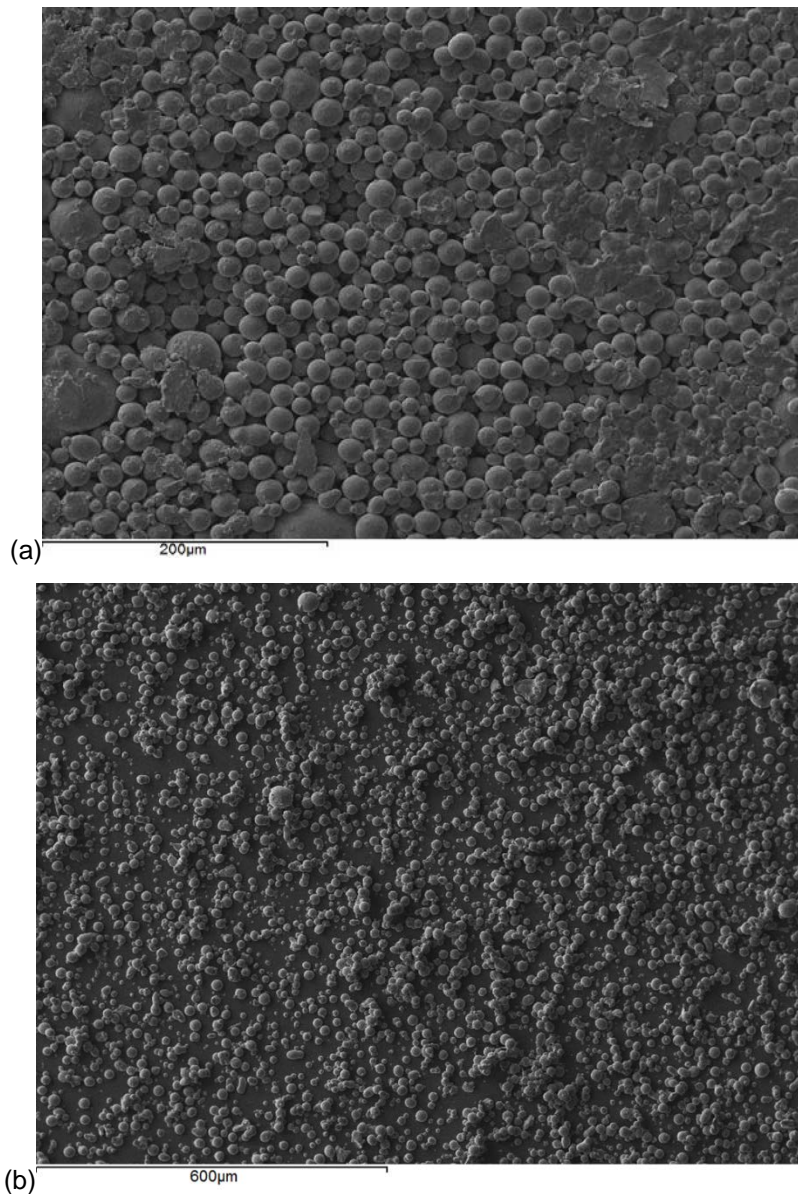244   (b)

245   Figure 5: (a) SEM image of the top surface of the pellet (b) SEM image of the separated micro-particles from

246   a pellet which is made of 40 mg/ml PVP concentration and fired at a pressure of 20 bar and separated using a

247   mesh of 178 μm pore size

248

249   **2.4 Modelling of micro-needle assisted micro-particle delivery: governing equations**

250   The detailed theoretical principle of each stage is discussed in the following sections.

251

252   **2.4.1   Acceleration stage**

253   For the MN assisted micro-particle delivery, a pellet is attached to a ground slide which is accelerated by a

254   pressurized gas in the acceleration stage (see Figure 1). It indicates that only the pressurized gas has done

255   the work during the acceleration process. The equation to describe this process:

$$E = \int_0^L P_2 \pi R^2 dl \qquad (1)$$

Where E is the kinetic energy of the pellet, L is the traveling distance of the ground slide in the barrel before the pellet is broken into micro-particles and R is the radius of the barrel. The gas pressure to push ground slide moving forward is P_2 which decreases from a pressure P_1 in front of the barrel. The gas expansion can be described by the Boyle's law (Webster, 1995) as below:

$$P_1 V_1^\gamma = P_2 (V_1 + V_2)^\gamma \qquad (2)$$

Where γ is the heat capacity ratio which defines as a constant of 1.6 for monatomic gas or 1.4 for diatomic gas.

The kinetic energy of the pellet attached ground slide at the end of the barrel can also be calculated as:

$$E = \frac{1}{2} M u^2 \qquad (3)$$

Where M is the mass of the pellet attached ground slide and u is the velocity of the ground slide.

From an energy conservation point of view, the ground slide velocity can be specified as follows:

$$u = \sqrt{\frac{2 P_1 V_1^\gamma [(V_1 + \pi R^2 L)^{1-\gamma} - (V_1)^{1-\gamma}]}{M(1-\gamma)}} \qquad (4)$$

2.4.2 Separation stage

In theory, the pellet is released from the ground slide at end of the barrel and separated by a mesh in the separation stage. Let us assume that the pellet has a mass of m_p and it is separated into n micro-particles with the same mass m and they have the same velocity u_1 after passing through the mesh. Further, the energy loss is assumed to be x in the process of the pellet separation. According to the energy conservation law to describe the kinetic energy of the separated micro-particles which is given as:

$$\frac{1}{2} n m u_1^2 = (1-x) \times \frac{1}{2} m_p u^2 \qquad (5)$$

The equation (5) can be rearranged to an equation which uses to calculate the velocity of the separated micro-particle and gives as:

$$u_1 = \sqrt{1-x} \times u \qquad (6)$$

2.4.3 Deceleration stage

The deceleration stage of the micro-particles is an important stage which directly affects the penetration depth of micro-particle in the skin. The drag force of the skin is the major factor to decelerate the micro-particles. In this work, the particle penetration in the skin use Newton's second law to proportional the change rate of particle momentum to the drag force f_d:

$$f_d = -m \frac{du_d}{dt} \qquad (7)$$

287 where f_d is the drag force acting on the micro-particles, u_d is the velocity of micro-particles.

288

289 Various studies have adopted that the drag force acting on the micro-particles is split into a yield force (F_y), a

290 frictional resistive force (F_f) and a resistive inertial force of target material (F_i) (Soliman et al., 2011; Liu, 2007;

291 Mitchell et al., 2003; Kendall et al. 2001; Dehn 1987). Thus, equation (7) is written as:

292
$$- (F_i + F_f + F_y) = m \frac{du_d}{dt} \tag{8}$$

293 The equations for each resistant force are shown as below:

294
$$F_i = 6\pi\mu_t r_p u_4 \tag{9}$$

295
$$F_f = \frac{1}{2}\rho_t A_c u_4^2 \tag{10}$$

296
$$F_y = 3A_c \sigma_y \tag{11}$$

297 Where μ_t is the viscosity of the target, r_p is the radius of the micro-particle, ρ_t is the density of the target and σ_y

298 is the yield stress of the target.

299

300 **2.5 Modelling strategy and parameters**

301 For the purpose of this paper, we use the software MATrix LABoratory (Matlab) to build and solve the

302 theoretical model for MN assisted micro-particle delivery. The model consists of three main parts including a

303 main program, an event program and two function programs (acceleration and deceleration stage). The main

304 program simulates the whole process of the MN assisted micro-particle delivery. The event program defines

305 the impact points of the micro-particles on the skin, rebound points on the boundary of the gap between mesh

306 and skin and the end points inside the skin. The function programs input the equations, which are used to

307 determine the theoretical results. The function programs are implemented to the main program by choosing a

308 suitable *ode* solver which requires considering the condition of the function program (stiff/non-stiff). In

309 addition, an *if* statement has been used to define the position of the micro-particles and further to confirm the

310 selection of the equations to calculate the theoretical velocity of micro-particles at different position. A *for*

311 statement has been used to repeat the simulation of a number of micro-particles in the deceleration stage.

312

313 In the model, human skin is considered as a target for micro-particles in the model. The three main layers of

314 human skin, stratum cornum (SC), viable epidermis (VE) and dermis layers are considered in the model. The

315 detailed skin properties are listed in the Table 2. It is worth to mention that the yield stress and density of the

316 dermis layer is considered the same with the viable epidermis layer. Zhang et al. (2014) have used porcine

317 skin instead of human skin to analyse the viscosity by using a rotational viscometer with parallel plate

geometry. The result will be used in this study, which is shown in Table 2. The viscosity of each skin layer is treated as the same in the model.

Table 2: Skin properties used in the model

Parameter	Value	Reference
Thickness of viable epidermis (VE), T_{ve} (m)	0.0001	Holbrook et al. (1974)
Thickness of stratum cornum(SC), T_{sc}(m)	0.00002	Matteucci et al. (2008); Schaefer et al. (1996)
Yield stress of SC , Y_{sc} (MPa)	3.2 - 22.5	Wildnauer et al. (1971)
Density of SC, ρ_{sc} (g/cm^3)	1.5	Duck (1990)
Density of VE, ρ_{ve} (g/cm^3)	1.15	Duck (1990)
Yield stress of VE, Y_{ve} (MPa)	2.2	Kishino et al. (1988)
Viscosity of skin, μ_t (Pa.s)	19.6	Zhang et al. (2014)

The lengths of the pierced holes are obtained from measuring the hole lengths in the skin mimicking agarose gel when MNs are inserted. In this case, this model is chosen to analyse the delivery of tungsten micro-particles. Zhang et al. (2014) have indicated that the pellet is separated into individual particles with a few agglomerates using a mesh and then penetrates into the target. It illustrates that a number of the tungsten particles agglomerated after the separation stage in the experiment. In order to correlate the model with the realistic experiments, a number of tungsten micro-particles are considered to the diameter of tungsten particle are considered to agglomerate together to be 3 μm diameter after the separation stage in the model. Previously, Zhang et al. (2013a,2014) have analysed the sauter diameter of the spherical and irregular stainless steel using a particle size analyser of Coulter. They also measured the average length of pierced holes in the skin mimicking agarose gel using a digital optical microscope. The length is considered uniformly and applied to the model in this case. The detailed set up of the particles properties and other relevant constants used in the model are listed in Table 3.

3. Results and Discussions

The purpose of this section is compare tungsten micro-particle with stainless steel micro-particles for the MN assisted micro-particle delivery based on the analysis of the passage percentage and the penetration depth inside target. The maximum penetration depth of micro-particles is analysed in relation to the operating pressure (see section 3.2.1) and MN length (see section 3.2.2). In addition, a theoretical model is used to analyse the penetration depth in relation to above two parameters to compare tungsten particle with stainless steel micro-particle and then to further understand the particle density effect on micro-particle penetration.

343 **Table 3**: Relevant constants used in the developed model

Parameter	Value
Mass of ground slide with the pellet, M (g)	1.25
Length of barrel, L(m)	0.5
Radius of barrel/ground slide, R(m)	0.00375
Volume of receiver, V_1 (L)	1
Space between mesh and skin, L_1 (m)	0.05
Density of tungsten (g/cm^3)	19.25
Density of stainless steel (g/cm^3)	8
Average Diameter of tungsten particle (µm)	3
Average Diameter of spherical stainless steel particle (µm)	18
Average Diameter of Irregular stainless steel particle (µm)	30
Viscosity of air, µ (Pa.s)	1.78
Length of pierced holes L_p(µm):	
Adminpatch 1500	1149
Adminpatch 1200	1048
In-house fabricated MN	656
Width of pierced holes L_w (µm):	
Adminpatch 1500	302
Adminpatch 1200	302
In-house fabricated MN	156

344

345 **3.1 Analysis of passage percentage**

346 In a previous study, Zhang et al. (2013a) have shown that stainless steel micro-particles yield a higher

347 passage percentage and a good quality size distribution of separated micro-particles if 40 mg/ml PVP (binder)

348 concentration and a mesh with pore size of 178 µm are used. Here, the pellets of tungsten micro-particles are

349 operated at the same conditions as the previous study of the stainless steel micro-particles and to make a

350 comparison of the passage percentage between those two micro-particles. The passage percentage is

351 analysed in relation to the operating pressure which is varied from 2.4 to 4.5 bar. As shown in Figure 6, the

352 passage percentage is increased due to an increase in the operating pressures for each micro-particle. This

353 is because the pellets gain more momentum at higher operating pressures, which in turn also causes the

354 separated particles to gain more momentum while passing through the mesh. Zhang et al. (2013a) have

355 indicated that the passage percentage of stainless steel micro-particles reaches a maximum due to some

356 particles sticking to the mesh and some rebounding, hence not passing into the test tube (particle collector).

357 As expected, the tungsten micro-particles show a similar performance to stainless steel. Figure 6 shows the

358 passage percentage of tungsten micro-particles is less significant than stainless steel micro-particles. It might

359 be the size of the tungsten particles is too small, which causes the velocity of the separated particles to

decrease faster after passage through the mesh and travel in air and stick on the mesh or the gap between mesh and target except the agglomerates.
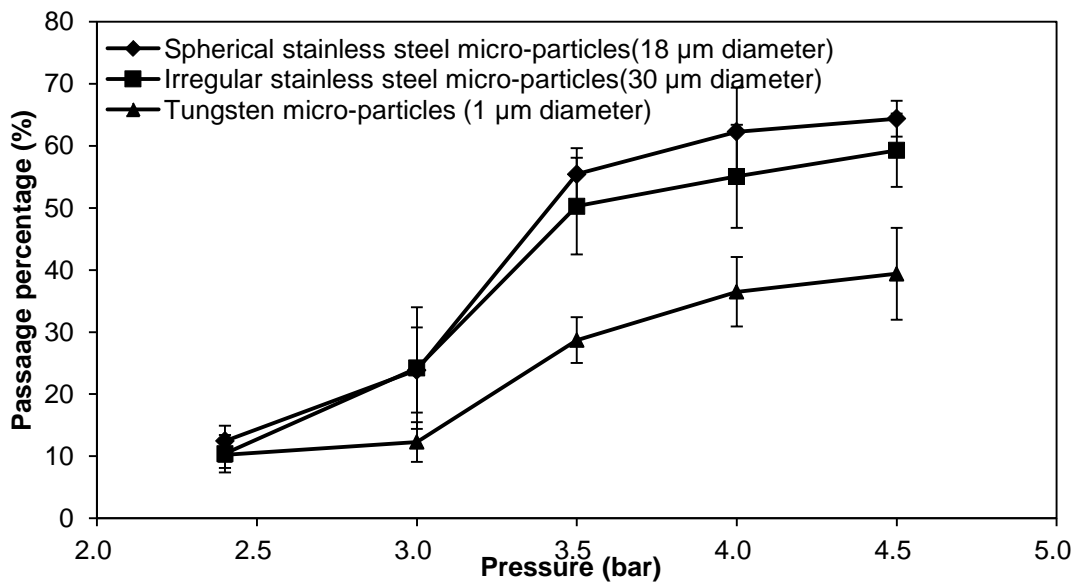
Figure 6: The effect of operating pressure on the Passage percentage of the pellet separation. Each curve in the figure is generated from three repeats of experiments (mesh pore size: 178μm, PVP concentration: 40 mg/ml)

3.2 Experimental analysis of the penetration depth of micro-particles

3.2.1 Effect of the operating pressure

The operating pressure is shown to be a key variable on the penetration depth of stainless steel micro-particles of 18 and 30 μm average diameters by us in a previous study (Zhang et al., 2013a, 2014). In this paper, we aim to investigate the difference of the penetration depth between the larger stainless steel micro-particle and smaller tungsten micro-particles at various pressures. The tungsten micro-particles cannot penetrate into the skin mimicking concentration of agarose gel. This is because the momentum of the particles is insufficient to breach the surface of the gel. In the experiment, the operating pressures are kept between 3 to 5 bar which are low for the small particles to achieve velocity to breach the target. It requires a higher pressure for the small particles to achieve sufficient momentum to penetrate further into the target. In addition, a comparison between tungsten and stainless steel micro-particles is shown in Figure 7. As can be seen, both irregular and spherical stainless steel particles of 30 and 18 μm average diameters achieve good penetration depths inside the skin mimicking agarose gel. Although the density of the stainless steel is lower than tungsten, larger diameters of stainless steel micro-particles increase their masses which lead to increased momentums of the micro-particles so as to allow them to penetrate further in the target (skin mimicking agarose gel). The two micro-particles show that the penetration depths increase due to an increase in the particle size.

385　To further understand the effect of the particle density and size on the penetration depth in the target, the

386　theoretical model is used to analyse the penetration of above two materials of micro-particles in a same target,

387　which is discussed in the section 3.3.2. When the MNs are inserted into the skin, it creates holes which

388　remain there after the removal of the MNs. The micro-particles can be delivered through these holes, thus

389　compensating for the insufficient momentum. As presented in Figure 7 the penetration depths of the tungsten

390　particles are greater inside the agarose gel when Adminpatch MN 1500 is used. This is because a number of

391　particles can penetrate through the pierced holes. However, the maximum penetration depths of the

392　micro-particles vary while the pressure increases from 3 to 5 bar. Zhang et al. (2014) have indicated that the

393　length of the pierced holes is unable to maintain constantly, which varies the maximum penetration depth of

394　the micro-particles inside the target. Thus, the variation in the length of the pierced holes directly affects the

395　penetration depth of the micro-particles. It means that the holes length is a major factor to maximize the

396　penetration depth in the MN assisted micro-particle delivery. The MN length effect on the micro-particle

397　penetration depth is discussed in the section 3.2.2 in detail. Figure 7 also shows that the penetration depths

398　of those two stainless steel micro-particles are more than the tungsten micro-particles. It indicates that an

399　increased momentum due to increase in particle size/operating pressure of micro-particles affect the

400　penetration depth in the MN assisted micro-particle delivery.

401

402　**3.2.2　Effect of the micro-needle length**

403　Zhang et al. (2014) have used three different lengths of MNs to study the maximum penetration depth

404　differences of stainless steel micro-particles of 18 and 30 μm diameters in a skin mimicking agarose gel. The

405　characterizations of those three MNs are presented in Table 1. To further determine the effect of MN length

406　on the penetration depth of small and dense micro-particles, those three MNs are used in this case. Figures

407　8a-b show the penetration of the tungsten micro-particles in the skin mimicking agarose gel based on the

408　assistance of Adminptach MN 1500 and the in-house fabricated MN 750, respectively. As can be seen, the

409　maximum penetration depth of micro-particles after using Adminptach MN 1500 is more than in-house

410　fabricated MN 750, but the number of micro-particles entering the pierced holes is less obvious. This is

411　because a long needle increases the length of pierced holes in the agarose gel, which maximizes the

412　penetration depth of micro-particles. In addition, the diameter of the in-house fabricated MN is greater than

413　the thickness of the Adminptach MN 1500 MN (see, Table 1), which creates wider holes to provide the

414　convenience for particle penetration. It indicates that a desired penetration depth and amount of

415　micro-particles can be controlled by changing the MN length and width for further research.
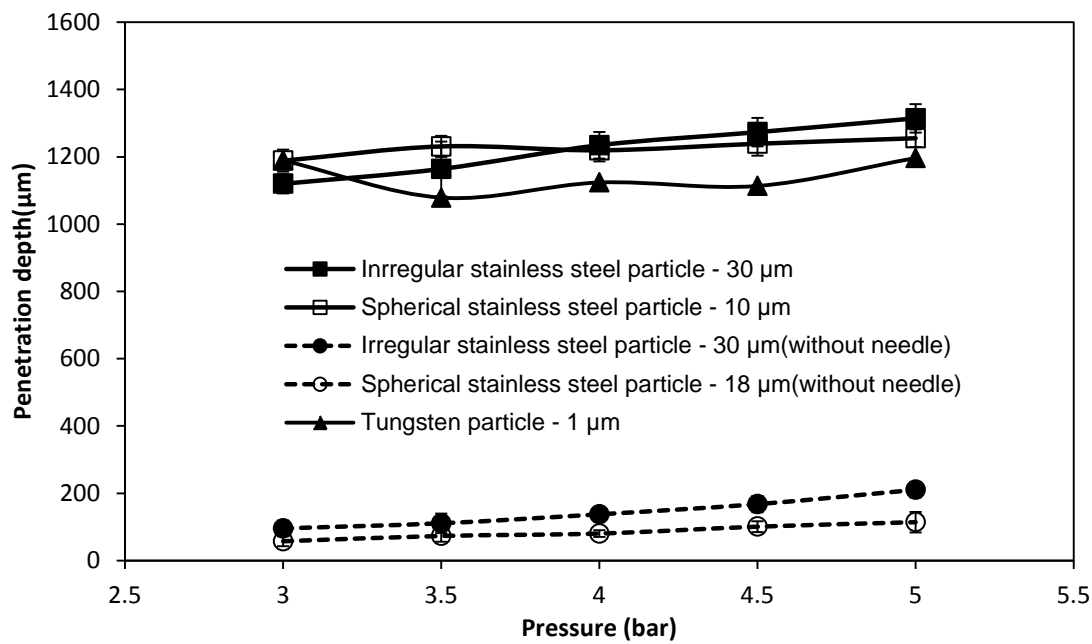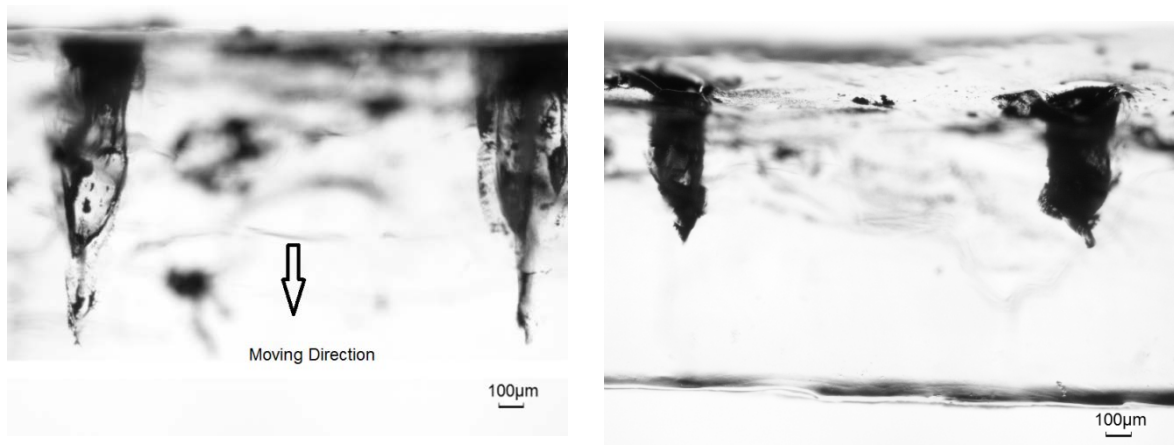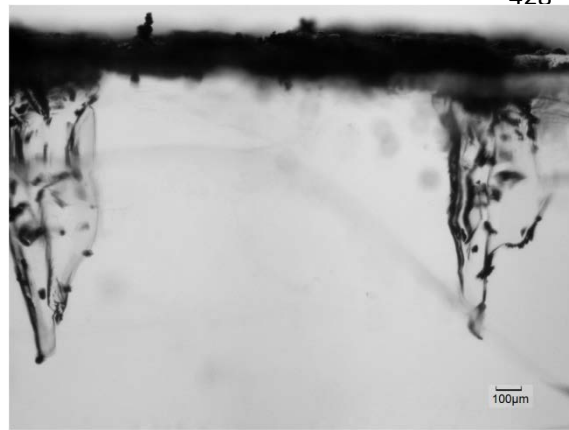
Figure 7: The effect of the operating pressure on the penetration depth of different type of particles (mesh: 178 µm of pore size: dash line: particle penetration without using MN; solid line: particle penetration with MN). Each curve in the figure is generated from three repeats of experiments.

(a)   (b)

Figure 8: The penetration of tungsten micro-particles in the skin mimicking agarose gel based on the assistance of MNs (a) Adminpatch MN 1500 (b) In-house fabricated MN 750

427

(a)   (b)

Figure 9: The penetration of stainless steel micro-particles in the skin mimicking agarose gel based on the assistance of MNs (a): spherical micro-particles of 18 µm average diameters (b): irregular micro-particles of 30 µm average diameters

Zhang et al. (2014) have fired spherical and irregular stainless steel micro-particles in the skin mimicking agarose gel. As presented in Figure 9, a number of micro-particles penetrated further through the pierced holes. It presents the same effect with the tungsten micro-particles. However, the amount of the stainless steel micro-particles that penetrates into the pierced holes is less than tungsten micro-particles if compared with the result in Figure 8. The number of irregular stainless steel micro-particles of 30 µm average diameter is less than spherical micro-particle (18 µm diameter) in Figure 9. It indicates that the amount of micro-particle in the pierced holes decreases from an increase in particle size. This is because of the hole is reformed after the removal of the MN, reduced the opening area of the hole on the top gel surface and further to affect the micro-particle penetration. Zhang et al. (2014) have shown that the thickness of the hole is only 78 µm after the removal of Adminpatch MN 1500. It limits the amount of the micro-particles to penetrate into the holes, especially to the large size of irregular stainless steel micro-particles. However, the maximum penetration depth of each micro-particle is close but related to length of the pierced holes.

The maximum penetration depths of tungsten micro-particles show significant differences between each MN array as shown in Figure 10. It increases from an increase in MN length. As expected, a longer MN increases the length of the pieced holes and thereby increases the maximum penetration depth of micro-particles. However, the maximum penetration depth is varied at different operating pressure. This is because the length of the pierced holes is varied after the removal of the MN array. The above results show the advantage of MN assisted micro-particle delivery which provides a positive effect on the particle penetration even if the momentum of the particle is insufficient to breach the target.
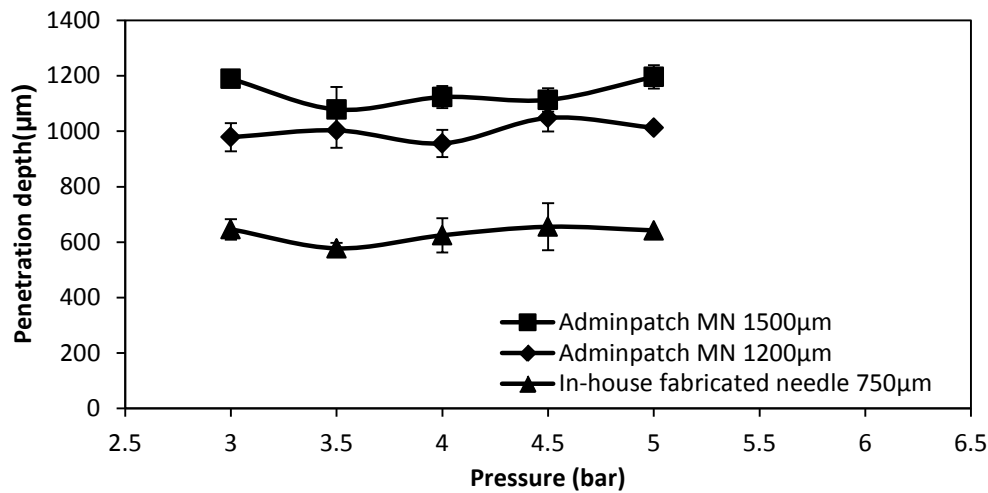
463 Figure 10: The maximum penetration depth of tungsten micro-particles in the skin mimicking based on the

464 assistance of MNs (mesh pore size: 178 μm; each curve in the figure is generated from three repeats of
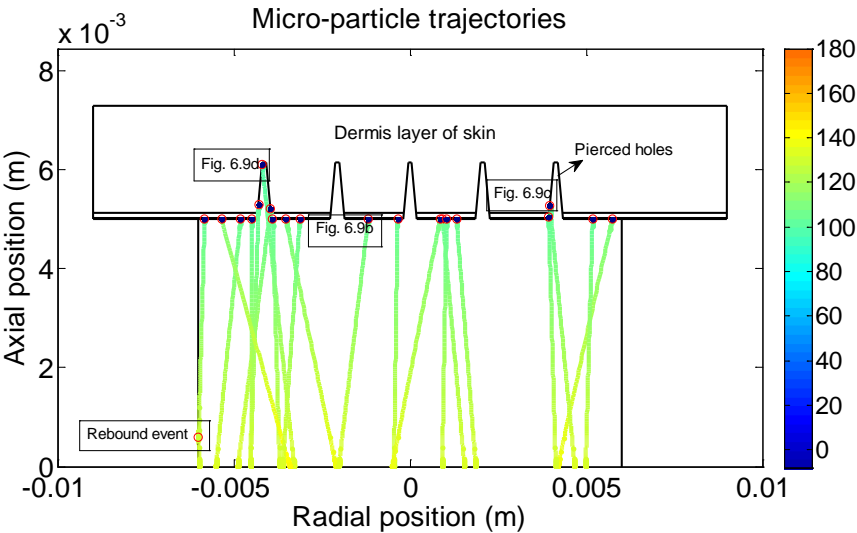
465 experiments).

466

467 **3.3 Modelling the penetration of micro-particle in skin**

468 Firstly, this section aims to understand the micro-needle assisted micro-particle delivery based on the

469 modelling of the trajectory of tungsten micro-particles in the deceleration stage. It is worth to mention that the

470 tungsten micro-particle and stainless steel micro-particle may vary in shape and size which may affect results

471 in reality. However, the both the stainless steel and tungsten micro-particles are assumed to be spherical with

472 uniform size (average diameter) in the model. The maximum penetration depth is analysed in relation to the

473 operating pressure, micro-needle length, particle size and density to further understand the difference

474 between tungsten and stainless steel micro-particles for the MN assisted micro-particle delivery. Finally, a

475 further analysis of the effect of each resistive force on the maximum penetration depth of micro-particles is

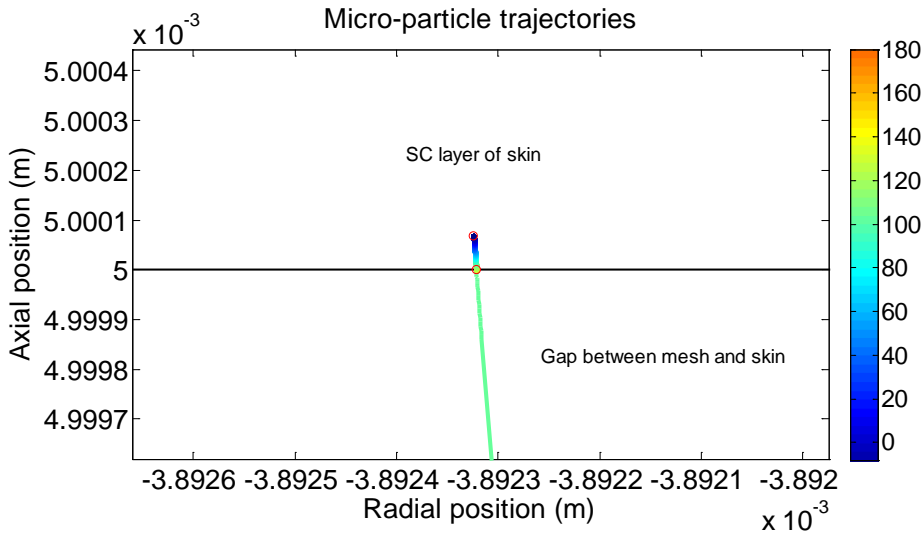476 discussed to verify the main factor which minimizes the penetration depth.

477

478 **3.3.1   Modelling the delivery of tungsten micro-particles**

479 Figure 11a shows the trajectories of increased diameter of tungsten micro-particles in the deceleration stage.

480 The initial positions of the micro-particles are randomly selected at the beginning to mimic the separation of

481 the pellet of tungsten micro-particles. In this case, we assumed that a number of tungsten micro-particles are

482 stuck together where the micro-particles are spherical in shape and each micro-particle has diameter of 3 μm

483 after the separation stage (mesh). The trajectory is considered to be linear. The velocity decrease is

484 represented by the colour change of the trajectory which corresponds to the colour bar in the figure. The

485 velocity decreases slowly from approximately 135 to 110 m/s from the mesh to the target. Figure 11a shows

486 that a number of the micro-particles achieve further penetration depths via the pierced holes. The figure

487 presents the similar performance of the developed model with experimental results. The detailed penetration

488 process of tungsten micro-particles in the skin are shown in Figure 11b-c. Figure 11b shows the penetration
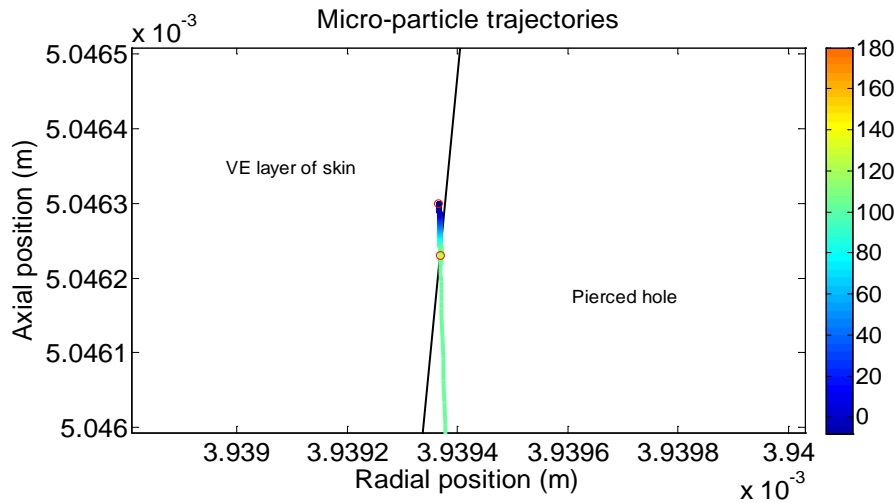
489   of tungsten micro-particles in the top skin layer of stratum corneum at 5 bar operating pressure. As can be

490   seen, the particle velocity deceases very fast in the stratum corneum due to an increased resistance; the

491   penetration depth is approximately 0.7 µm which could be ignored. Some particles are delivered through the

492   pierced holes and then penetrate into the epidermis/dermis layer of the skin (side surface of the pierced

493   holes), as shown in Figure 11c. It shows that the variation of the velocity is changed slightly in the pieced

494   holes and decreased fast after penetrating the skin. It shows a similar performance as the penetration in the

495   stratum corneum due to an increased resistance. Based on the above figures the penetration depth of

496   tungsten micro-particles is negligible in the skin, which matches well with the experimental results.

497   .(a)

498

499   (b)

Micro-particle trajectories

500 (c)

501 Figure 11: The trajectories of the tungsten micro-particles in the deceleration stage: (a). The overall view of

502 the micro-particle trajectories (b).The particle penetration at the area without needle hole (c).The view of the

503 micro-particle penetrate through the needle hole (pressure: 5 bar)

504

505 **3.3.2   The effect of the operating pressure and particle size on the penetration depth**

506 In the experimental results, the operating pressure only presents a slight effect on the penetration depth of

507 the tungsten micro-particle without using MN. The pressures are varied from 3 to 5 bar, which are too low for

508 small micro-particles when compared with previous gene gun research (Arora et al., 2008; Giudice et al.,

509 2006; Kendal et al., 2004; Mitchell et al., 2003). In order to further understand the effect of the operating

510 pressures on the penetration depth of this tungsten micro-particle, the penetration depth is analysed at

511 various operating pressures which range from 3 to 60 bar in the model. As presented in Figure 12 the

512 penetration depth of the tungsten particle is increased from 0.04 to 0.28 μm without using MNs while the

513 pressure varies from 3 to 60 bar. The penetration depth is negligible. It illustrates that the tungsten particle of

514 3 μm diameter are too small for penetration even if the operating pressure increases to a great value. Figure

515 12 also shows the tungsten particle achieves a great penetration depth after using MNs. However, the

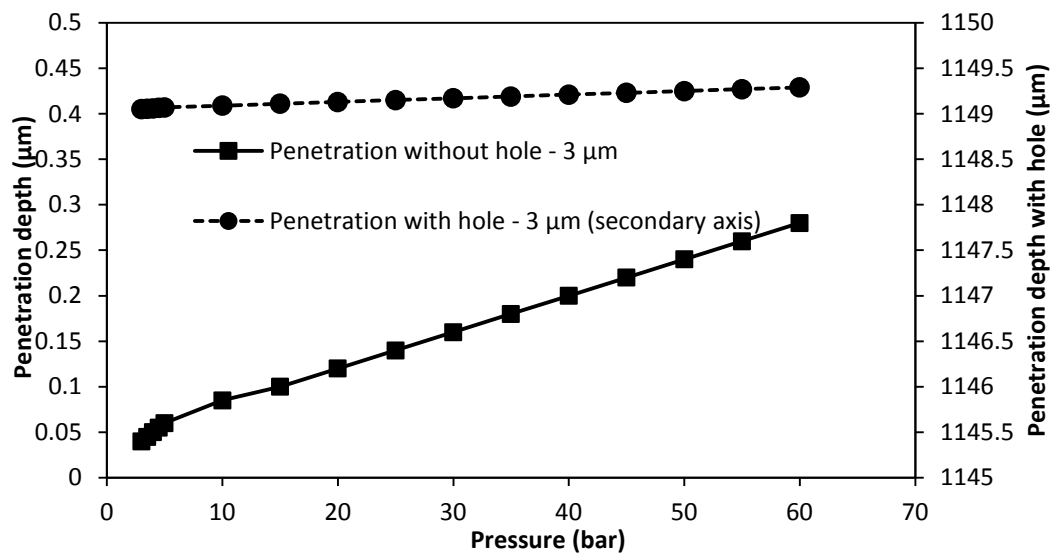516 penetration depth is increased slightly from an increase in operating pressure.

517

518

519   Figure 12: The effect of the operating pressure on the penetration of tungsten particle

520

521   To further understand the effects of particle size and density on the penetration depth, the particle is assumed

522   to be spherical in shape with uniform size and the particle diameter is varied from 3 to 100 μm for both

523   stainless steel and tungsten micro-particles using the presented model. As presented in Figure 13 the

524   penetration depth of tungsten micro-particles increases from 0.07 to 65.61 μm in the skin without using MNs

525   and from 1149.07 to 1214.61μm using Adminpatch MN 1500 at 5 bar pressure. It shows more penetration

526   depth than stainless steel which only penetrates 0.02 to 17.36 μm in the skin and 1149.02 to 1170.5 μm using

527   a same MN as tungsten while the particle diameter ranges from 3 to 100 μm. This comparison directly shows

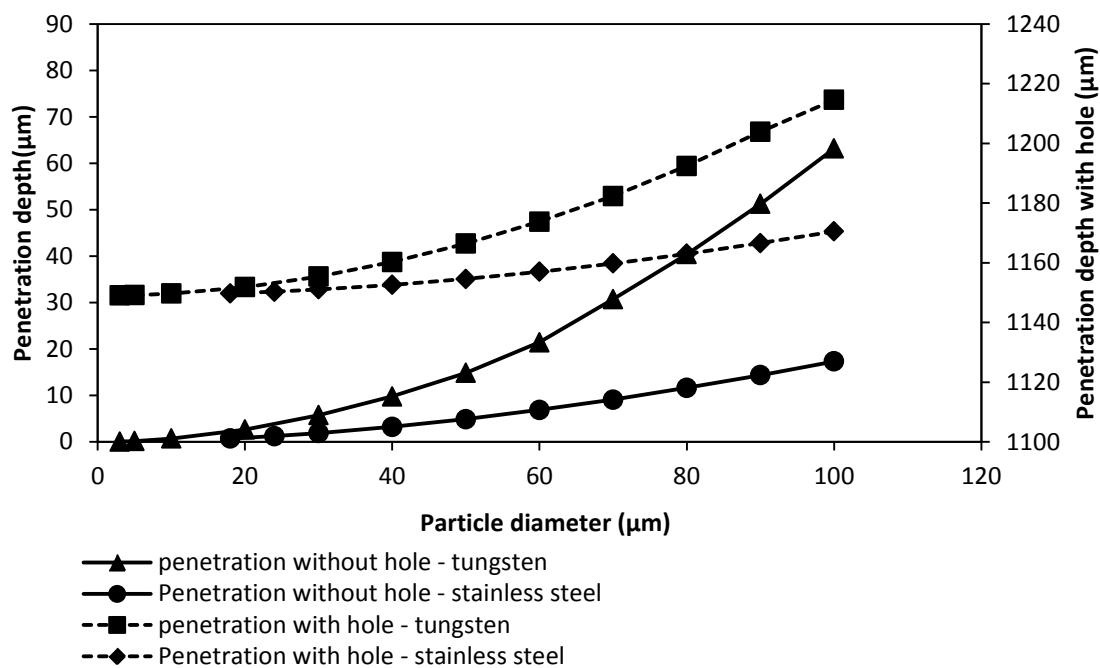528   the advantage of dense particles on the penetration in the target for gene gun systems.

529

530   Figure 13: The effect of the tungsten particle size on the penetration depth (operating pressure: 5 bar)
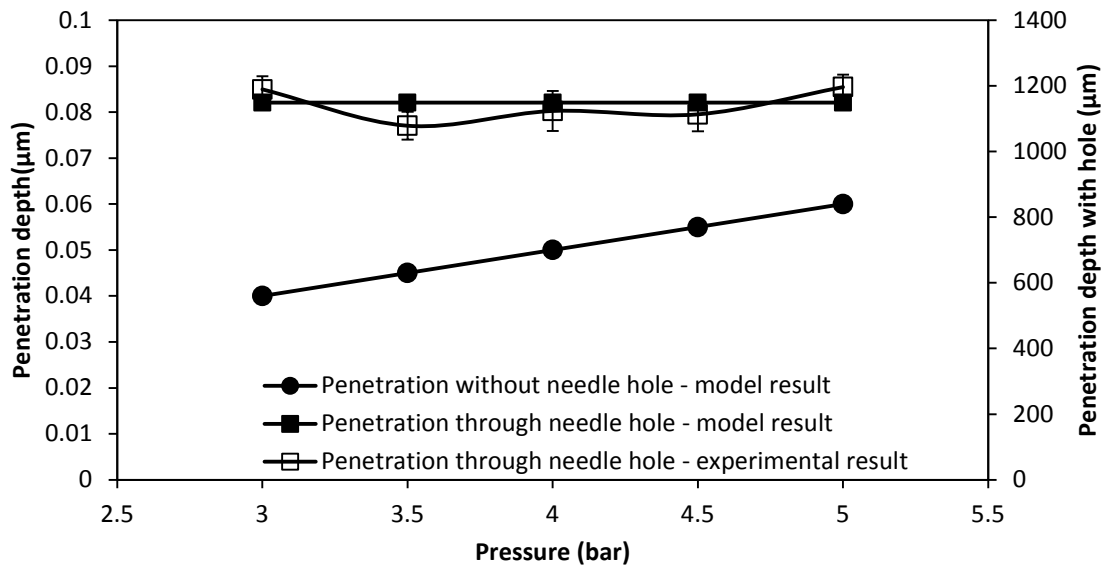
531

Figure 14: A comparison of penetration depth between model and experimental results (particle type: tungsten micro-particle of 3 μm diameter). The experimental results in the figure are generated from three repeats of experiments.

A comparison of the penetration depth of the tungsten micro-particles (3 μm) between model and experimental results is shown in Figure 14. It is worth to mention that the difference between experiment and modelling may be due to the assumption that the particle shape of the tungsten particle is regular after the separation stage in the model. As can be seen, the tungsten particles penetrate less than 0.1 μm without using MN for the model result. It matches well with the experimental results which show the tungsten micro-particles cannot penetrate into the skin mimicking agarose gel. However, this condition can be made up by using MNs. As presented in Figure 14 the tungsten micro-particles reaches a further depth using Adminpatch MN 1500, but the maximum penetration depths are varied at pressure ranges from 3 to 5 bar. This is because it is not possible to ensure that the length of the pierced holes is constant each time using the same MN. As expected, the model results match well with the experimental results. In conclusion, the maximum penetration depth of tungsten micro-particles is directly related to the length of the pierced holes, and the operating pressure only presents a slight effect on the penetration depth in this case. To further understand the effect of pierced holes on the penetration depth of tungsten micro-particles, three different lengths of MNs (see Table 1) have used and discussed in the following section.
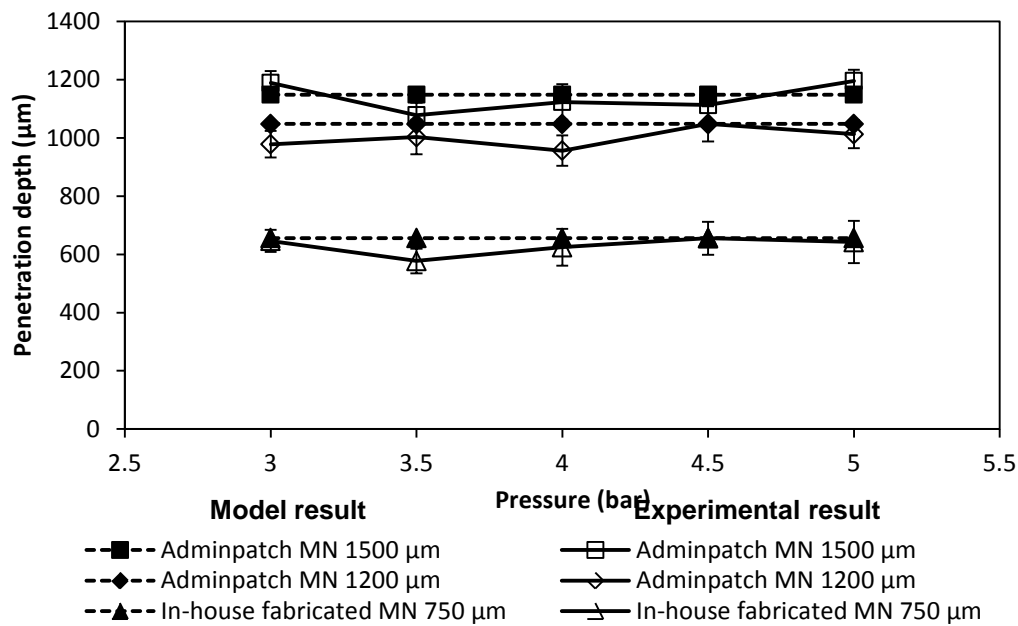
Figure 15: The effect of the micro-needle length on the maximum penetration depth of the tungsten particle (operating pressure: 5 bar; particle type: tungsten micro-particle of 3 μm diameter). The experimental results in the figure are generated from three repeats of experiments.

3.3.3 The effect of the micro-needle length

In the real experiments, some tungsten micro-particles may be agglomerate after the separation stage. However, any effects of the particle agglomeration on the model results are not accounted for directly at this moment. This may be the reason why there are some differences between the experimental and modelling results; however, all comparison have produced reasonable match between the experimental and modelling results. Zhang et al. (2014) have shown that the length of pierced holes has a greater effect on the maximum penetration of stainless steel particles, which is related to the MN length. As expected, it agrees with the results of tungsten micro-particles shown in the Figure 15. As can be seen, the maximum penetration depth of tungsten micro-particles seems to be increased with an increase in the MN length. In principle, the length of pierced holes is directly related to the MN length which maximizes its length. An increased length of the pieced holes allows a number of micro-particles which deliver into the holes to penetrate further inside the target and maximizes the penetration depth. As expected, the experiment results are varied for each application of MNs due to difficulties maintaining a constant hole length. However, the model results match well with the experimental results, which illustrate the applicability of the model for MN assisted micro-particle delivery.

3.3.4 Dependence of particle penetration depth to particle size and density in relation to the resistive forces in the dermis layer of the human skin

The skin properties vary with one person to another (e.g., gender, age, race and various anatomical areas of

the body of the same person (Xu et al., 2007; Vexler et al., 1999). As discussed earlier, the penetration depth of micro-particles is related to the yield force (F_y), a frictional resistive force (F_f) and a resistive inertial force of target material (F_i) which decelerate the high-speed micro-particles inside the target (see equation 8). However, the yield force depends on the yield stress of the target (equation 11). Further, the resistive inertial force is related to the target viscosity (equation 9) and the frictional resistive force depends on the density of the target material (equation 10). In view of these inter-dependencies which in turn affect the micro-particle delivery, this section aims to analyse the effects of each force on the penetration depth of micro-particle to further investigate the major factors which provide a greater effect on the penetration depth.

For the MN assisted micro-particle delivery, the main point is the maximum penetration depth of the micro-particle in the skin. As discussed already, a number of the micro-particles penetrate through the holes made by the MNs to the dermis layer of the skin. In order to investigate the effect of each force on the maximum penetration depth of micro-particle, we assume that the micro-particles penetrate into the dermis layer at the tip area of the hole to obtain the maximum penetration depth of micro-particles. In addition, we kept one of those three resistive forces as constant and ignored the other two forces to analyse the variation of the penetration depth in the model. As shown in Figure 16, stainless steel micro-particles penetrated further than the tungsten particles due to the difference in particle size. Figure 16 also shows that the frictional resistive force provided a minimum effect on the micro-particle penetration. The effect of the yield force on the penetration depth is greater than the frictional resistive force. However, the major factor is the resistive inertial force which causes the penetration depth of micro-particles is almost negligible if the hole length (1149 μm) is subtracted.

As discussed earlier, the resistive inertial force is a major component that determines the penetration depth of micro-particles for the gene gun based micro-particle delivery. Target viscosity directly affects the resistive inertial force. In order to further understand the effect of the resistive inertial force on the particle maximum penetration depth, the theoretical model is used to simulate the effect of varying the viscosity of the dermis layer from 5 to 19.6 MPa where we kept the yield stress and density (see Table 2) and the hole length constant and operated the system at 5 bar operating pressure. As presented in Figure 17, the maximum penetration depth decreased from an increase in viscosity of the dermis layer. This is because an increased resistive inertial force slows down the particle velocity rapidly. Figure 17 also shows that the effect of a decreased viscosity of dermis layer on the maximum penetration depth is increased from an increase in particle size and density due to an increased momentum. The maximum penetration depth of small micro-particle (tungsten particle of 3 μm diameter) is kept to approximately a constant when the viscosity of dermis layers is changed.
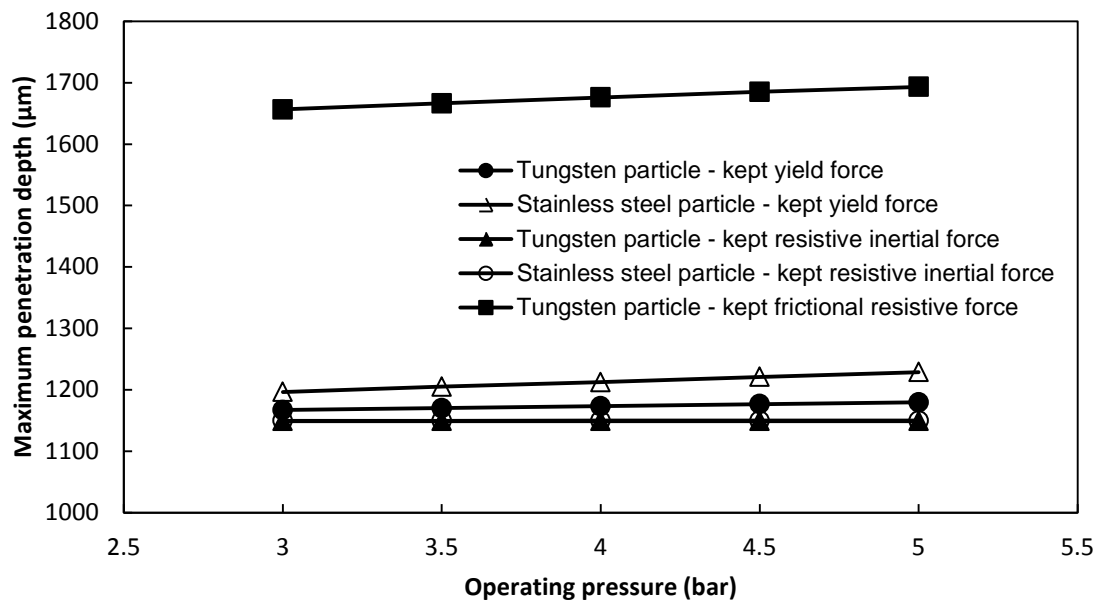
Figure 16: The effect of each resistive force on the maximum penetration depth of micro-particles (stainless steel particle: 18 µm diameter; tungsten particle: 3 µm diameter; Hole length: 1149 µm)

3.3.5 Further Discussions

A comparison between stainless steel and tungsten micro-particles on the penetration depth in the skin mimicking agarose gel has been made in this study. Tungsten micro-particles are unable to penetrate the skin mimicking agarose gel/skin without using MN in the experimental result, which is different from the results of stainless steel micro-particles. The reason is that the diameter of tungsten micro-particles is less than 1 µm which is too small when compared with the stainless steel micro-particles of 18 and 30 µm diameters. As a result the momentum of the tungsten micro-particles is too low to allow the particles to breach the gel surface. Zhang et al. (2013a) have measured the velocity of ground slide, which only reaches around 122 m/s at 5 bar pressure, using a photoelectric sensor, which means that the particle velocity is less due to the energy loss. This velocity is less than some previous studies for gold particles, e.g., Kendal (2001) has shown that 1 ± 0.2 µm diameter gold particles can reach a velocity of 580 ± 50 m/s at 40 bar pressure using a contoured shock tube (CST). The ground slide presents a significant negative effect on the particle velocity, but it has safety advantage which prevents the pressurized gas from impacting the human body. Thus, the operating pressure is mimicked from 3 to 60 bar to study the penetration differences of tungsten micro-particles after increasing the momentum in the theoretical model. However, the tungsten micro-particles still cannot achieve the expected penetration depth. It indicates that a ground slide based gene gun system is not useful for the intercellular route because micro-particles cannot reach velocities high enough to breach the skin. Increasing the particle size will increase the moment but cause damage to the surface of the skin. As a result the extracellular route is the expected solution for normally ground slide based gene gun system.
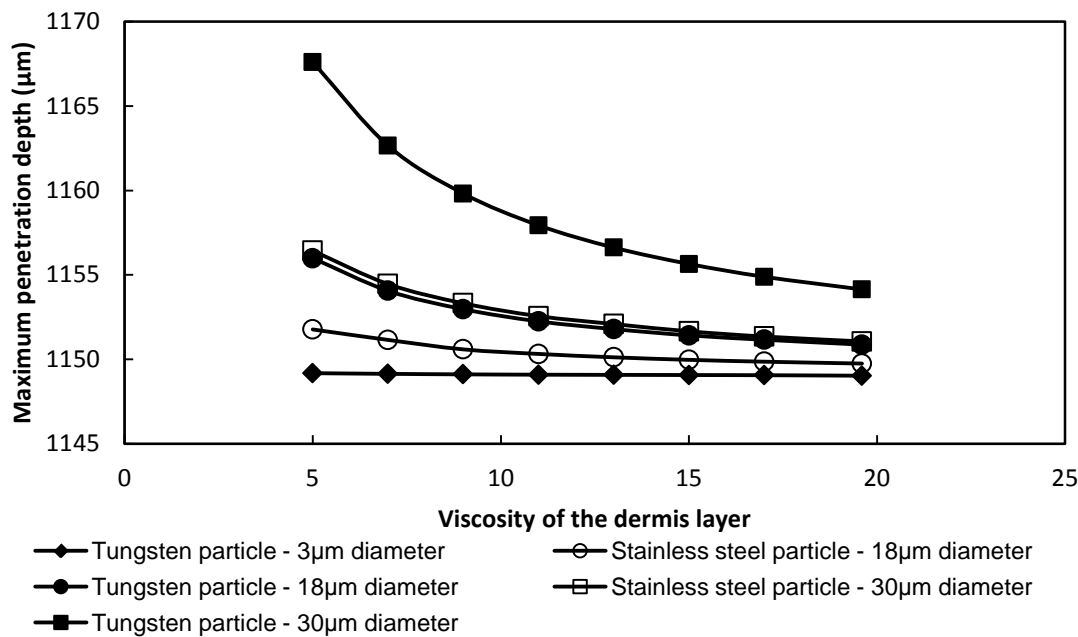
Figure 17: The effect of the viscosity of dermis layer on the maximum penetration depth of micro-particles (operating pressure: 5bar; hole length: 1149 µm)

However, the use of MN meets the purpose of an intercellular route to deliver micro-particle to a greater penetration depth in the target using a ground slide based gene gun system. Previously, Zhang et al. (2013a) have shown that the penetration depth of stainless steel micro-particles is increased while using a MN. In this paper, the tungsten micro-particles are investigated using modelling and experiments with MN assisted micro-particle delivery. Both model and experimental results show that the use of MN increases the penetration depth of tungsten micro-particles. However, the maximum penetration depth of micro-particles depends on the length of pierced holes which is created by MNs. The maximum penetration of tungsten micro-particles reaches around 1149 µm using Adminpatch 1500 MM, which has possibly never reached for other relevant gene gun systems. For example, Kendal (2001) has indicated that gold particles of 1 ± 0.2 µm diameters can penetrate 66 µm in the skin at velocity of 580 ± 50 m/s using a contoured shock tube (CST). Kendal et al. (2004) have also used a convergent-divergent device to accelerate 1.8 µm diameter gold particles which achieves a maximum penetration depth of 78.6 µm at 60 bar. Mitchell et al. (2003) has shown that gold particles of 1-3 µm diameters can reach a maximum depth of around 60 µm in canine tissue at a velocity of 550 ± 50 m/s. It is concluded that the diameters of gold particles ranges from 1 to 3 only can penetrates to a depth from 60 to 78.6 µm (epidermis layer) which is less than the maximum penetration depth of the tungsten particles after using MNs. It shows that the improvement of the penetration depth using MN assisted micro-particle delivery, which achieves depths never reached before. In conclusion, the results show that the intercellular route is feasible for the MN assisted micro-particle delivery. In theory, it is the preferred route for MN assisted micro-particle delivery due to the cell damage is minimized from a decrease in particle size (O'Brien et al., 2011), although extracellular route presents more penetration depth. It could be proved by firing the above stainless steel/tungsten micro-particles into cell cultured skin mimicking agarose gel to

659 analyse the cell damage in further work. Future work should also focus on using animal/human skin for

660 detailed histological studies in contrast to agarose gel as used in this study. If using the proposed methods,

661 one should also be aware of the likeliness of dermal damage and pain that may occur if using long

662 microneedles besides any effect of gene gun on mechanical damage of the skin. Therefore, safety studies

663 should be conducted in detail in future studies.

664

4. Conclusions

666 This study shows an effective method for relating the use of MNs to create holes on the target for

667 micro-particle delivery to improve the penetration depth of micro-particles. The experimental rig considers

668 possible changes in the operating pressure to analyse the penetration depth and passage percentage of

669 tungsten and stainless steel micro-particles. Results show that the passage percentage increases due to an

670 increase in operating pressure until a maximum value. Tungsten micro-particles used in this study present a

671 lower passage percentage than stainless steel due to an insufficient momentum to reach the target (particle

672 collector). In addition, tungsten micro-particles are stopped by the skin mimicking agarose gel even if the

673 operating pressure is increased. But an increased operating pressure improves the penetration of stainless

674 steel particle without using MNs. This is because the diameter of tungsten micro-particles is small (< 1 μm).

675 To further understand the particle size and density effect on the penetration depth, a theoretical model is used

676 to mimic the operating pressure ranges from 3 to 60 bar to accelerate tungsten and stainless steel

677 micro-particles while the diameter ranges from 3 to 100 μm. The results show a great improvement in the

678 penetration depth of tungsten micro-particles which is more than stainless steel micro-particles. However,

679 both model and experimental results show that a use of MNs provides an improvement on the penetration

680 although the momentum is insufficient to breach the skin. The maximum penetration depth of micro-particles

681 up to dermis layer has not been reached before. It is related to length of MNs which determine the length of

682 pierced holes. As expected, model results matches well with the experimental results, which illustrates the

683 applicability of the model for the MN assisted micro-particle delivery. MN assisted micro-particle delivery

684 improves safety because an intercellular route can be chosen to reduce the damage from particle impact and

685 the pressurized gas is prevented by the ground slide. In addition, it also enhances the penetration depth of

686 micro-particles properly if compared with any other gene gun systems. An increased penetration depth allows

687 deeper tissue to be transfected, which provides more effective gene transfection in the target. Future work

688 could be to attach the genes on the micro-particles, fired into the cells using MN assisted micro-particle

689 delivery and then analyse the DNA profile of the cells to verify the advantage of MN assisted micro-particle

690 delivery.

691

695   Muddimer, Mr Terry Neale and Mr Steve Bowler are acknowledged.

696

697   **6. Conflict of Interest**

698   The authors declare no conflict of interest

699

700   **7. References**

701   Al-Qallaf B., Das D.B., Davidson A., (2009). Transdermal Drug Delivery by Coated Microneedles: Geometry

702   Effects on Drug Concentration in Blood, *Asia-Pacific Journal of Chemical Engineering*, **4**(6): 845-857, DOI:

703   10.1002/apj.353.

704

705   Arora A., Prausnitz M.R., Mitragotri S., (2008) Micro-scale devices for transdermal drug delivery, *Int. J. Pharm.*

706   **364**: 227-236

707

708   Bastian S., Busch W., Kuhnel D., Springer A., Holke R., Scholz S., Pompe W., Gelinsky M., Potthoff A.,

709   Richter V., Ikonomidou C., Schirmer K., (2009). Toxicity of tungsten carbide and cobalt-doped tungsten

710   carbide nanoparticles in mammalian cells in vitro, Environ. *Health Perspect*,**117**(4): 530-536

711

712   Bennett A.M., Phillpotts R.J., Perkins S.D., Jacobs S.C., Williamson E.D., (1999). Gene gun mediated

713   vaccination is superior to manual delivery for immunisation with DNA vaccines expressing protective antigens

714   from Yersinia pestis or Venezuelan Equine Encephalitis virus, *Vaccine*, **18**(7-8): 588-596

715

716   Crozier W.D., Hume W., (1957). High velocity light gas gun, *Journal of Applied Physics*, **28**(8): 892-895

717

718   Cormier M., Johnson B., Ameri M., Nyam K., Libiran L., Zhang D. D., and Daddona P.. (2004). Transdermal

719   delivery of desmopressin using a coated microneedle array patch system. *J. Control. Release*, **97**: 503-511

720

721   Davis S.P., Landis B.J., Adams Z.H., Allen M.G., Prausnitz M.R.. (2004). Insertion of microneedles into skin:

722   measurement and prediction of insertion force and needle fracture force, *Journal of Biomechanics*, **37**:

723   1155-1163.

724

725   Dehn J. (1987). A Unified theory if penetration, *International journal of impact engineering*, **5**: 239-248

726

727   Duck F.A. (1990). Physical Properties of Tissue: A Comprehensive Reference Book, London: Academic

728   Press, Harcourt Brace Jovanovich

729

730   Donnelly R.F., Garland M.J., Singh T.R.R., Migalska K., Majithiya R., McCrudden C.M., Kole P.L., Mahmood

731   T.M.T., McCarthy H.O., Willfson A.D. (2012). Hydrogel-Forming microneedle array for enhanced transdermal

732   drug delivery, *Adv. Funct. Mater.*, **22**:4879-4890.

733

734   Vexler A., Polyansky I., Gorodetsky R., (1999). Evaluation of skin viscoelasticity and anisotropy by

735   measurement of speed of shear wave propagation with viscoelasticity skin analyser, *Journal of Investigative*

736   *Dermatology*, **113**: 732-739

737

738   Giudice E.L., Campbell J.D., (2006). Needle-free vaccine delivery, *Adv.Drug Deliv. Rev.* **58:** 68-89

739

740   Han T., Das D.B. (2013). Permeability enhancement for transdermal delivery of large molecule using

741   low-frequency sonophoresis combined with microneedles, *Journal of Pharmaceutical Science*, **102**(10):

742   3614-3622

743

744   Hardy M.P., Kendall M.A.F., (2005). Mucosal deformation from an impinging transonic gas jet and the ballistic

745   impact of micro-particles, *Phys. Med. Biol.*, **50**: 4567-4580

746

747   Holbrook, K. A., Odland, G.F. (1974). Regional Differences in the thickness (cell layers) of the human stratum

748   corneum: an ultrasound analysis, *J Invest Dermatol.*, **62**: 415-422.

749

750   Kalluri H., Banga A.K.. (2011). Formation and closure of microchannels in skin following microporation,

751   *Pharm. Res.*, **28**: 82-94

752

753   Kendall M.A.F., Carter F.V., Mitchell T.J., and Bellhouse B.J., (2001). Comparison of the transdermal ballistic

754   delivery of micro-particle into human and porcine skin, *Proceedings of the 23rd Annual International*

755   *Conference of the IEEE*: 2991-94

756

757   Kendall M.A.F., Rishworth S., Carter F., Mitchell T., (2004). Effects of relative humidity and ambient

758   temperature on the ballistic delivery of micro-particles to excised porcine skin, *J. Invest. Dermatol.* **122**:

759   739-746.

760

761   Kis E.E., Gerhard W., Myschik J., (2012). Devices for intradermal vaccination, *Vaccine*, **30**: 523-538

762

763   Kishino A., Yanagida T., (1988). Force measurements by micromanipulation of a single actin filament by glass

764   needles, *Nature*, **334**: 74-76

765

766 Klein T.M., Wolf E.D., Wu R. and Sanford J.C., (1987). High-velocity microprojectiles for delivering nucleic
767 acids into living cells, *Nature*, **327**: 70-73

769 Liu Y., (2006). Physical-mathematical modelling of fluid and particle transportation for DNA vaccination,
770 *International Journal of Engineering Science*, **44**: 1037-1049

772 Liu Y., (2007). Impact studies of high-speed micro-particle following biolistic delivery, IEEE transactions of
773 biomedical engineering, *Transactions on Biomedical Engineering*, **54**(8): 1507-1513

775 Macklin, M.D., Drape, R.J., Swain, W.F., (2000). "Preparation for particle-mediated gene transfer using the
776 Accell gene gun", *Methods in molecular medicine*, **29**: 297-303

778 Matteucci, M., Fanetti, M., Casella, M., Gramatica, F., Gavioli, L., Tormen, M., Grenci, G., De Angelis, F., Di
779 Fabrizio, E. (2009) Poly vinyl alcohol re-usable masters for MN replication. *Microelectronic Engineering*,
780 **86**(4-6): 752-756 doi:10.1016/j.mee.2009.01.068

782 McAllister D.V., Wang P.M., Davis S.P., Park J.H., Canatella P.J., Allen M.G., Prausnitz M.R.. (2003).
783 Microfabricated needles for transdermal delivery of macromolecules and nanoparticles: fabrication methods
784 and transport studies. *PNAS*, **100**: 13755–13760

786 Menezes V., Mathew Y., Takayama K., Kanno A., Hosseini H., (2012). Laser plasma jet driven microparticles
787 for DNA/drug delivery, *PLOS ONE*, **7**(11): e50823

789 Mitchell T.J., Kendall M.A.F., Bellhouse B.J., (2003). A ballistic study of micro-particle penetration to the oral
790 mucosa, *International Journal of Impact Engineering*, **28**: 581-99

792 Miyano T., Tobinaga Y., Kanno T., Matsuzaki Y., Takeda H., Wakui M., and Hanada K., (2005). Sugar micro
793 needles as transdermic drug delivery system. *Biomed. Microdevices*, **7**: 185-188

795 Nayak A., Das D.B. (2013). Potential of biodegradable microneedles as a transdermal delivery vehicle for
796 lidocaine, *Biotechnology Letters*, **35**(9): 1351-1363

798 Nayak A., Das D.B., Vladisavljević, GT (2013). Microneedle-Assisted Permeation of Lidocaine
799 Carboxymethylcellulose with Gelatine Co-polymer Hydrogel. Pharmaceutical Research, DOI:
800 10.1007/s11095-013-1240-z (in press)

802   O'Brien J.A., Lummis S.C.R., (2011). Nano-biolistics: a method of biolistic transfection of cells and tissues

803   using a gene gun with novel nanometer-sized projectiles, *BMC Biotechnology*, **11**; 66

804

805   Olatunji, O., Das, D.B. (2010). Painless Drug delivery using microneedles. Current technologies to increase

806   the transdermal delivery of drugs (Editor: Joan Escober Chavez). *Bentham Science Publishers* (available

807   online at http://www.benthamdirect.org/pages/b_getarticlebybook.php). ISBN:978-1-60805-191-5.

808

809   Olatunji, O., Das, D.B. (2011). Drug delivery using Microneedles. Comprehensive Biotechnology (Editor:

810   Zhanfeng Cui). 2nd Edition, MS number 501. MRW, Elsevier, The Boulevard, Langford Lane, Oxford, United

811   Kingdom. ISBN: 13: 978-0-444-53352-4

812

813   Olatunji, O, Das, DB, Nassehi, V (2012) Modelling transdermal drug delivery using microneedles: Effect of

814   geometry on drug transport behaviour, *Journal of Pharmaceutical Sciences*, **101**(1): 164-175, ISSN:

815   0022-3549. DOI: 10.1002/jps.22736.

816

817   Olatunji O., Das D.B., Garland M.J., Belaid L., Donnelly R.F., (2013).   Influence of Array interspacing on the

818   force required for successful microneedle skin penetration: theoretical and practical approaches, *Journal of*

819   *Pharmaceutical Science*, **102**(4): 1209-1221.

820

821   Quinlan N.J., Kendall M.A.F., Bellhouse B.J., Ainsworth R.W., (2001). Investigations of gas and particle

822   dynamics in first generation needle-free drug delivery device, *Shock Waves*, **10**: 395-404

823

824   Ritman E.L., (2004). Micro-computed tomography – Current status and developments, *Annual review of*

825   *Biomedical Engineering*, **6**: 185-208

826

827   Russell J.A., Roy M.K., Sanford J.C., (1992). Physical trauma and tungsten toxicity reduce the efficiency of

828   biolistic transformation, *Plant Physiol.*, **98**: 1050-1056

829

830   Sato H., Hattori S., Kawamoto S., Kudoh I., Hayashi A., Yamamoto I., Yoshinari M., Minami M., Kanno H.,

831   (2000). In vivo gene gun-mediated DNA delivery into rodent brain tissue, *Biochem. Biophys. Res. Commun.*,

832   **270**(1): 163-170.

833

834   Schaefer, H., Redelmeier, T.E. (1996) Skin barrier: Principles of percutaneous absorption, New York, Karger.

835

836   Soliman S.M. (2011). Micro-particle and Gas Dynamics in an Axi-symmetric Supersonic Nozzle, University of

837   Cincinnati (Cincinnati, USA), *Thesis for the degree of Doctor of Philosophy in Aerospace Engineering.*

838

839 Soliman S.M., Abdallah S., (2011). CFD investigation of powdered vaccine and gas dynamics in biolistic gun,

840 *Powder Technology*, **214**: 135-142

841

842 Soliman S.M., Abdallah S., Gutmark E., Turner M.G., (2011). Numerical simulation of microparticles

843 penetration and gas dynamics in an axi-symmertric supersonic nozzle for genetic vaccination, *Powder*

844 *Technology*, **208**: 676-783

845

846 Thomas J.L., Bardou J., Mauchamp B. et al, Chavancy Gerard (2001). A helium burst biolistic device adapted

847 to penetrate fragile insect tissues, *Journal of Insect Science*, **1**(9): 1-10

848

849 Trainer A.H., Alexander M.Y., (1997). Gene delivery to the epidermis, *Human molecular genetics*, **6**(10):

850 1761-1767

851

852 Uchida M., Li X.W., Mertens P., Alpar H.O., (2009). Transfection by particle bombardment: Delivery of

853 plasmid DNA into mammalian cells using gene gun, *Biochim. Biophys. Acta.*, **1790**(8):754-764

854

855 Walters K.A., Roberts M.S., (2007). Dermatologic, Cosmeceutic, and Cosmetic Development, Therapeutic

856 and Novel Approaches, CRC press, Chapter 36: 591-611

857

858 Webster C., (1995). The Discovery of Boyle's law, and the concept of the Elasticity of Air in the Seventeenth

859 Century. *Arch. Hist. Exact Sci.*, **2**: 441-502

860

861 Wildnauer R.H., Bothwell J.W., Douglas A.B., (1971). Stratum corneum properties I. Influence of relative

862 humidity on normal and extracted stratum corneum, *J. Invest. Dermatol.*, **56**: 72-78

863

864 Williams R.S., Johnston S.A., Riedy M., DeVit M.J., McElligott S.G., Sanford J.C., (1991). Introduction of

865 foreign genes into tissues of living mice by DNA-coated microprojectiles, *Proc. Natl. Acad. Sci. U.S.A.*, **88**:

866 2726-2730

867

868 Xu F., Wen T., Seffen K.A., LuT.J., (2007). Characterization of Thermomechanical behaviour of skin tissue –

869 Viscoelastic behaviour, *Proceedings of the World Congress on Engineering*, **2**: WCE 2007

870

871 Yoshida Y., Kobayashi E., Endo H., Hamamoto T., Yamanaka T., Fujimura A., Kagawa Y., (1997). Introduction

872 of DNA into rat liver with a hand-held gene gun: Distribution of the expressed enzyme, [32P] DNA, and Ca2+

873 flux, *Biochem. Biophys. Res. Commun.* **234**(3): 695 -700.

874

875 Yoshimisu Y., Tanaka K., Tagawa T., Nakamura Y., Matsuo T., Okamoto S., (2009). Improvement of

876 DNA/Metal Particle Adsorption in Tungsten-Based Biolistic Bombardment; Alkaline pH is Necessary for DNA

877 Adsorption and Suppression of DNA Degradation, *Journal of Plant Biology*, **52**: 524-532.

878

879 Zhang D.W., Das D.B., Rielly C.D., (2013a). An experimental study of microneedles assisted micro-particle

880 delivery using a model system, *Journal of Pharmaceutical Science*, **102**(10): 3632-3644, DOI:

881 10.1002/jps.23665.

882

883 Zhang D.W., Das D.B., Rielly C.D., (2013b). Potential of microneedles assisted micro-particles delivery from

884 gene gun: A review. *Drug Delivery*, DOI: 10.3109/10717544.2013.864345 (in press).

885

886 Zhang D.W., Das D.B., Rielly C.D., (2014). Microneedles assisted micro-particles delivery from gene guns:

887 Experiments using skin mimicking agarose gel. *Journal of Pharmaceutical Sciences*, DOI: 10.1002/jps.23835

888 (in press).